



CHORUS

This is the accepted manuscript made available via CHORUS. The article has been published as:

Non-Gaussianity in single-particle tracking: Use of kurtosis to learn the characteristics of a cage-type potential

Pavel M. Lushnikov, Petr Šulc, and Konstantin S. Turitsyn

Phys. Rev. E **85**, 051905 — Published 14 May 2012

DOI: [10.1103/PhysRevE.85.051905](https://doi.org/10.1103/PhysRevE.85.051905)

Non-gaussianity in single particle tracking: use of kurtosis to learn the characteristics of a cage-type potential

Pavel M. Lushnikov¹, Petr Šulc², and Konstantin S. Turitsyn³

¹ *Department of Mathematics and Statistics, University of New Mexico, Albuquerque, NM, 87131, USA*

² *Rudolf Peierls Centre for Theoretical Physics, University of Oxford, Oxford OX1 3NP, UK*

³ *Department of Mechanical Engineering, Massachusetts Institute of Technology, Cambridge, MA, 02139, USA*

Nonlinear interaction of membrane proteins with cytoskeleton and membrane leads to non-Gaussian structure of their displacement probability distribution. We propose a statistical analysis technique for learning the characteristics of the nonlinear potential from the time dependence of the cumulants of the displacement distribution. The efficiency of the approach is demonstrated on the analysis of the kurtosis of the displacement distribution of the particle traveling on a membrane in a cage-type potential. Results of numerical simulations are supported by analytical predictions. We show that the approach allows robust identification of some characteristics the potential for the much lower temporal resolution compared with the mean square displacement analysis and we demonstrate robustness to experimental errors in determining the particle positions.

PACS numbers: 87.80.Nj, 87.16.dp, 05.40.-a, 02.70.Rr

Rapid progress in video-capturing, sub-diffractive microscopes and fluorescence technologies has transformed a single particle tracking (SPT) technology in a powerful tool for studying the properties of biological environments and complex fluids [1]. In a typical experiment some specific type of biomolecule, i.e. protein or lipid, is labeled by a fluorophore or a nanoparticle, and its motion is tracked with a camera in subdiffractive resolution [2]. The abundance of data available from the SPT experiments has risen demand in data analysis techniques that would help scientists to characterize the interaction of particle with the environment based on the statistical properties of particle trajectories. Many of the currently used approaches rely on the analysis of second order moments, like the mean square displacement (MSD) [1]. The main objective of this Letter is to demonstrate the potential of other statistical properties that go beyond Gaussian approximation and second-order correlations. In a practically interesting example of a protein moving on the membrane we show that many characteristics of the particle-membrane interactions that cannot be recovered from the analysis of MSD reveal themselves as distinct statistical signatures in the time dependence of the kurtosis of the particle displacement distribution. These signatures are supported by analytical predictions. The non-Gaussianity of jumps observed during anomalous diffusion has been recognized for many years (see e.g. the review [3]), however, to our knowledge the problem of connecting the non-Gaussianity with the structural properties of the environment is still open. In addition, the analysis of the kurtosis of the particle displacements ignoring the time-dependence gives quite limited information [4] contrary to our approach which relies of distinct properties of time dependence.

The motion of proteins and lipids within biological membranes plays important role in many biological processes. Previous assumption that biological membrane can be considered as two-dimensional fluid with freely diffusing lipids and proteins [5, 6] are now significantly al-

tered by the experimental observations that membranes are highly heterogeneous [7, 8]. Models of lipid rafts, pickets and fences, protein-protein complexes and protein islands were suggested [9–12]. According to these models the motion of the location and diffusion of membrane proteins are significantly influenced by the domains of different lipid or protein compositions (lipid rafts, protein islands) as well as by the interaction with the cytoskeleton and anchored transmembrane proteins (form fences and pickets, respectively). E.g., the compartmentalization of the plasma membrane is perhaps the best explained by the fences and pickets [10]. Inside each compartment proteins (lipids) experience fast diffusion (at time scales $\lesssim 0.01s$ [10]) which agrees well with the diffusion in the artificial membranes (which do not have cytoskeleton). A hopping between different compartments (jump over fences) occurs at larger time scale $\tau_h \sim 0.01s$. (see e.g. Table 2 in Ref. [10] for the specific values of τ_h for several types of cells).

Most SPT studies have been relying on the standard video rate (~ 30 frames/sec) [1] which does not allow a detailed resolution of the fast diffusion inside compartments because the inter-compartment hopping rate $1/\tau_h$ exceeds the video rate. The exceptions are Kusumi [10] and Ritchie [13] groups which use $25\mu s$ and $1ms$ temporal resolutions, respectively. The analysis of SPT trajectories in the significant majority of previous work has been based on the analysis of MSD [1]. It was demonstrated that SPT with the standard video rate is not sufficient to recover any details about fast diffusion inside compartments as well as any information about compartments [10]. MSD uses only a small part of information about properties of particle trajectories. The only exception when MSD is optimal corresponds to the pure random walk of the particle when probability distribution of particle displacement is Gaussian. However, any inhomogeneity on plasma membrane (represented e.g. by the inhomogeneous potential) results in the non-Gaussianity of that probability distribution which makes MSD non-

optimal to recover the properties of the system from the SPT trajectories.

In parallel to biology SPT based approaches were developed in microfluidics under the name of microrheology [14]. Tracking of the Brownian motion of individual particles immersed in viscoelastic fluid allows reconstruction of viscoelastic modulus from the Laplace transform of particle MSD. To our knowledge, all common variations of microrheology (including two-particle and active microrheology) are based on the analysis of second-order correlation functions, and assume linear response of the viscoelastic fluid. Although microrheological settings are not described in this Letter, the methods discussed below can be naturally applied there.

A number of other techniques have been proposed for identification of the potentials on biological membranes based on the analysis of individual trajectories. Most comprehensive approach is to solve the inverse problem of reconstruction of $U(\mathbf{r})$, $\mathbf{r} = (x, y)$ from the trajectories. However, such problem is generally ill-posed [15] and needs very large statistics of trajectories. E.g., Ref.[16] suggested to infer forces acting on the biomolecule [17] requiring the multiple particle visits of each spatial location which is difficult to achieve experimentally. In addition, the potential U in living cells can slowly change with time. This fact may limit the application of inverse problem approaches, that attempt to reconstruct the specific potential. Another approach [10, 18] focuses on identification of the potential barriers from MSD-based analysis. That approach is successful but requires very high temporal resolution of trajectories. Ref. [4] used the kurtosis to analyze the displacements relative to the center of gravity of the particle trajectory. Such definition of the kurtosis looks only into the spatial distribution of visited points, thus completely ignoring the time-dependence which is in sharp contrast with the approach that we will use. Refs. [19–21] used fourth order moment to infer the properties of anomalous diffusion. One more method is based on the measurement of autocorrelation of SPT trajectories and recovering of the probability distribution of particle jumps [22] which indirectly displays the information about the inhomogeneity of the plasma membrane. In contrary, the technique analyzed in this Letter has more modest goals of learning the characteristic scales associated with the potential. It does not rely on long observations of individual particles, and can be based on aggregation of time-series from an ensemble of measurements of different particles in the same class of membranes.

In this Letter we propose to recover major features of the potential from SPT trajectories using the time-dependence of the kurtosis as the measure of non-Gaussianity. We demonstrate by the combination of numerical and analytical methods that the rate ~ 100 frames/sec might be sufficient for that purpose far superior to the performance of MSD-based methods.

The starting point of our work is the following observation. Whenever a particle experiences nonlinear interactions, for example with the cytoskeleton, the proba-

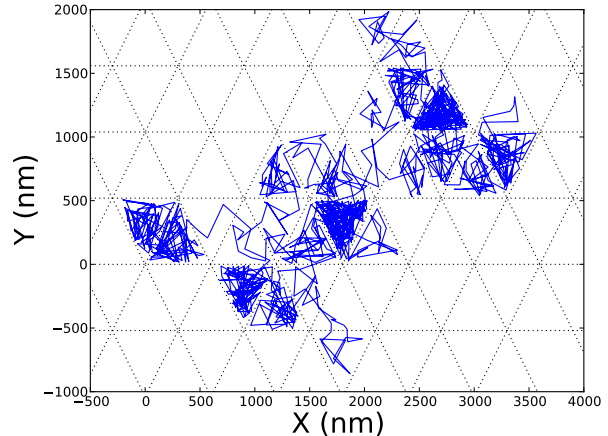


FIG. 1: (Color online) Simulation of the trajectory of a diffusing protein in triangular compartments of size 600 nm during 10 seconds shown with a time resolution 10 ms. The dashed lines indicate the borders between compartments.

bility distribution of the particle displacement becomes non-Gaussian. Therefore, analysis of the deviations from Gaussian distribution can reveal new information about the nonlinear interactions. There is a infinite number of characteristics that measure the degree of non-Gaussianity, because the nonlinear interaction can take infinite number of forms. In this Letter we consider only one of the characteristics, that can be accurately estimated with limited amount of time-series data. Kurtosis of the particle displacement distribution, defined as

$$K_{\alpha}(t) = \frac{\langle [\Delta r_{\alpha}(t) - \langle \Delta r_{\alpha}(t) \rangle]^4 \rangle}{3 \langle [\Delta r_{\alpha}(t) - \langle \Delta r_{\alpha}(t) \rangle]^2 \rangle^2} - 1. \quad (1)$$

Here $\Delta r_{\alpha}(t) = r_{\alpha}(t) - r_{\alpha}(0)$ is the α component of the particle displacement, and $\langle \dots \rangle$ denotes the time average along the particle trajectory as well as it might mean additional ensemble average over several simulations (when we mention that explicitly below). If the probability distribution of particle displacement is Gaussian, the kurtosis will be equal to zero for any time interval t . Kurtosis of the displacement distribution originates from the nonlinear interactions of the particle with the environment, and as shown below, incorporates a lot of information about the structure of these interactions.

We model the motion of the particle using the Monte Carlo algorithm (see e.g. [17]) as a two-dimensional (2D) random walk on an elementary triangular lattice composed of equilateral triangles with side length $a = 1$ nm (or $a = 0.25$ nm in the case of the inset in Figure 2). The membrane compartments are typically modeled as equilateral triangles filling entire 2D plane with sides of length $L = 300$ nm, 150 nm and 600 nm. In separate simulations we also considered random distortions of these triangles as well as rectangles filling 2D plane. The potential energy on the elementary lattice site i is labeled as U_i . Figure 1 shows the typical simulation of total time 10 s. In

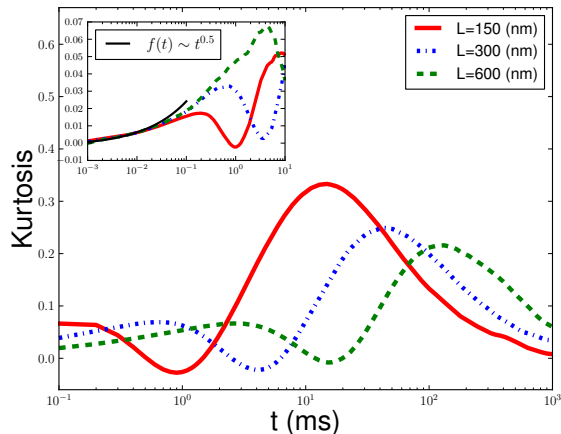


FIG. 2: (Color online) The kurtosis of the displacements along x for 3 different compartment sizes calculated with the resolution $0.1ms$. The inset shows the kurtosis scaled as $1/L$ for the resolution $1\mu s$ and a function $f(t) \approx t^{1/2}$ (thin black line) which shows that the kurtosis scales as $t^{1/2}$ for small t

each simulation step, a random closest neighbor j of site i that is occupied by the random walker (diffusing protein) is chosen. The move to site j from i is accepted with probability $p = \min(1, \exp[(U_i - U_j)/T])$. We set the temperature $T = 1$. The potential of barriers between compartments is defined as $U_i(l) = H \exp(-d_{i,l}^2/\sigma^2)$, where $U_i(l)$ is the contribution to the total potential U_i at site i from l th barrier and $d_{i,l}$ is the distance from site i to l th barrier. U_i is given by the sum of contributions from all barriers: $U_i = \sum_l U_i(l)$. Also H is the height of the barrier and the width of the barrier is 2σ . By default the barrier parameter σ is set to 5 nm and $H = 7$. But for the inset of Figure 2, we model a higher barrier with $\sigma = 8$ nm and $H = 10$.

We set the diffusion coefficient to $D = 2.5\mu m^2 s^{-1}$ on the lattice, which means that one iteration step of the MC simulation corresponds to a time period $\tau = 0.1\mu s$ for lattice size $a = 1nm$ and $\tau = 0.00625\mu s$ for $a = 0.25nm$ according to the relation $D = a^2/(4\tau)$. Effect of the discretization is negligible at time scales $\gg \tau$ which motivates our choice of the numerical values of a .

For $U_i \equiv 0$ the particle experiences a Brownian motion with $\langle \Delta x^2 + \Delta y^2 \rangle = 4Dt$ and $K(t) = 0$. However, if U is nonzero, the kurtosis of the particle motion acquires a non-trivial shape as shown in Figure 2 for three different compartment sizes. The typical length of simulation was 10^9 steps with every 10^3 -th step recorded, thus corresponding to an experiment of total length $100s$ with a time resolution (i.e. inverse frame rate) 0.1 ms. Note that we always use the elementary time step τ to generate particle trajectories. Experimental observations have much lower temporal resolution than τ and to imitate such resolution we use only a small fraction of simulation points to calculate the kurtosis for each chosen resolution. Figure 2 shows that the kurtosis is characterized

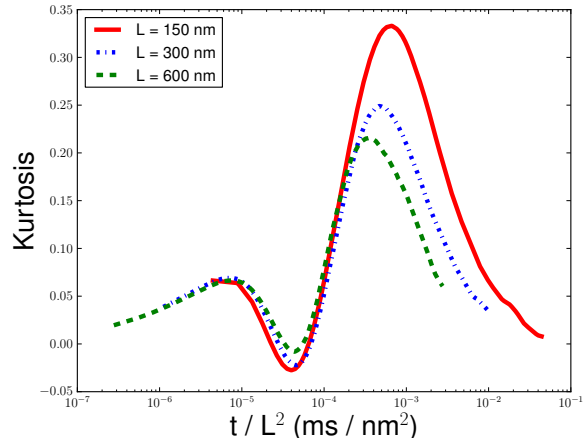


FIG. 3: (Color online) The kurtosis for three different compartment sizes L as a function of rescaled time t/L^2 showing L^2 scaling of the position of the minima. The time resolution of each simulation was $0.1ms$ and total length was 10^4s .

by two peaks separated by a local minima. The inset of Figure 2 shows a simulation with lattice size $a = 0.25nm$, the duration $10s$ and the resolution $1\mu s$, which we used to test the analytical predictions for kurtosis behavior for low times as discussed below. The kurtosis in that inset is divided by L . The kurtosis scales as $1/L$ for low times t and grows as $t^{1/2}$, as expected from our analysis. Figure 3 shows that the position of the minima scales as L^2 as also expected from our analysis below.

The kurtosis of simulations with three different temporal resolutions $0.1ms$, $1ms$ and $10ms$ for the compartment size $L = 300$ nm are shown in Figure 4. Already for the resolution $\simeq 10ms$ it is possible to see the characteristic features of the kurtosis inferring compartments' structure by comparing with the pure diffusion case. The kurtosis curves are averaged over 5 different simulation runs, each of duration $100s$ for the resolution $0.1ms$ and $500s$ for the resolutions $1ms$ and $5ms$. We also show the kurtosis for pure diffusion simulations, which should be equal to 0 for the infinite trajectory. The error bars show standard deviation for the five simulations with the resolution $0.1ms$. The inset compares MSD of pure diffusion with no barriers and two different simulations with the resolutions $0.1ms$ and $10ms$ for $L = 300nm$. While the MSD plot with the resolution $0.1ms$ shows transition from the fast diffusion regime inside the compartment with $D = 2.5\mu m^2 s^{-1}$ to the slow hopping diffusion regime with $D = 0.1\mu m^2 s^{-1}$, the MSD plot of $10ms$ resolution is able to capture only the slow diffusion.

Figure 5 shows that the kurtosis is quite robust to the defects of the triangular compartment lattice which we demonstrated by randomly removing different percentage of barriers. We also found similar robustness when we randomly distorted equilateral triangular lattice by 10% in angles compare with $\pi/3$ angles as well as when we used rectangular lattice instead of triangular one. An-

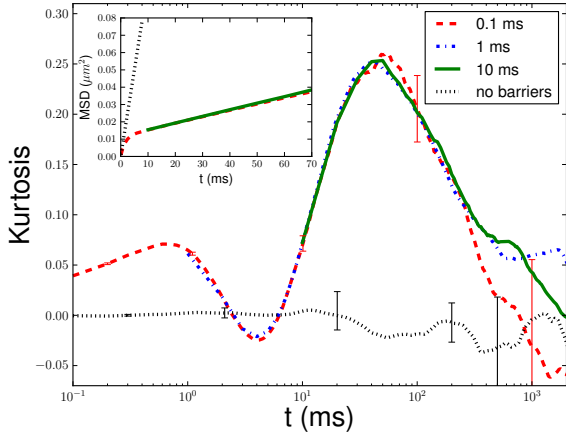


FIG. 4: (Color online) The kurtosis along x for 3 different resolutions with $L = 300$ nm. The kurtosis for pure diffusion (no barriers) is also shown with the resolution 0.1 ms. Error bars correspond to 0.1 ms resolution. The inset shows MSD for diffusion with no compartments (short dashed line) and for simulations with the resolutions 0.1 ms (long dashed line) and 10 ms (solid line).

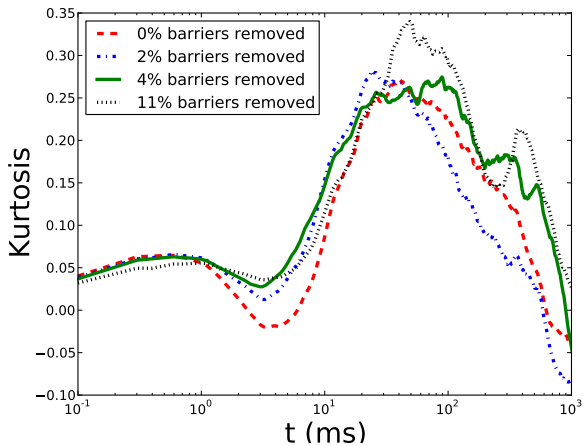


FIG. 5: (Color online) The kurtosis along x for different fractions of randomly removed barriers for simulation of 100s duration for triangular compartments with $L = 300$ nm and 0.1 ms resolution.

other important measure is the sensitivity to the experimental noise in the position of particles. We checked that the kurtosis is quite robust for the noise up to $\simeq 30$ nm in the position of particles as shown in Figure 6.

Observed structure of the kurtosis time dependence $K(t)$ can be explained theoretically in a limiting case when the characteristic time $\tau_d \sim L^2/D$ associated with the diffusion inside the compartment is much smaller than the hopping time τ_h between consecutive hopping over the barrier. To estimate τ_h we solve the Smolu-

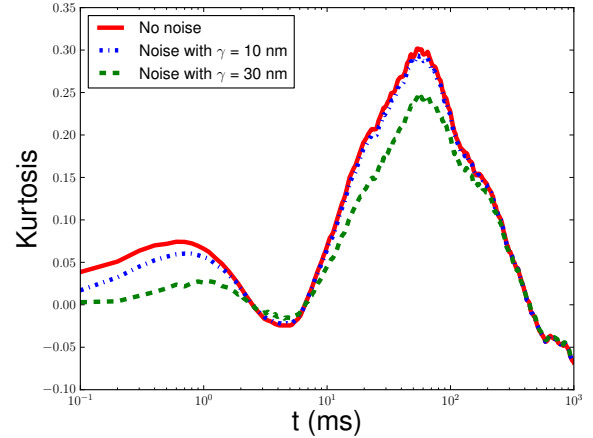


FIG. 6: (Color online) The kurtosis along x for different levels of the simulated experimental noise (simulated as the error in the measurement of particle position) in position of particles for simulation of 100s duration and the same parameters as in Figure 5. The simulated noise is taken to be Gaussian with the variance γ^2 .

chowski equation

$$\partial_t p = D \nabla \cdot [p \nabla U + \nabla p] \quad (2)$$

for the time-dependent probability density function (PDF) $p(\mathbf{r}, t)$ of the particle position \mathbf{r} . Constant-flux solution of (2) in the adiabatic approximation $\partial_t p \simeq 0$ (valid because $\tau_h \gg \tau_d$) gives the relation between the flux of the probability through the barrier $\propto -Dp'(0)$ and the jump $p(0^+) - p(0^-)$ of PDF between compartments:

$$p(0^+) - p(0^-) = p'(0) \mathcal{P}^{-1}, \quad (3)$$

where the barrier is assumed to be infinitely thin (i.e. $\sigma/L \ll 1$), $p(0^+)$ and $p(0^-)$ are values of p from different sides of the barrier, $p'(0) \equiv \mathbf{n} \cdot \nabla p$ is the normal derivative of p at the barrier and \mathbf{n} is the normal unit vector to the barrier. For the Gaussian form of the barrier the permeability \mathcal{P} is given by $\mathcal{P} = H^{1/2} \pi^{-1/2} \sigma^{-1} e^{-H}$ resulting in $\tau_h \sim \mathcal{P}^{-1} L D^{-1} \sim \tau_d (\sigma/L) H^{-1/2} e^H$.

The initial rise of the kurtosis function $K(t)$ in the region $t \ll \tau_d$ is related to short trajectories that experienced some nonlinear interaction. As the only source of nonlinearity in this model is the interaction with the barrier, they correspond to reflections from the barrier. The short length of the trajectories in this region of t allows one to explain this behavior via analysis of a simplified problem of one-dimensional diffusion in the neighborhood of reflecting wall. Assuming that the random walk takes place in the x direction, the Green function which is defined as a probability density of the final position $x = X(t)$ assuming that the particle was at position x_0 at $t = 0$ is given by $2G(x; x_0, t) = G_0(x - x_0; t) + G(x + x_0; t)$, where

$G_0(x; t) = (2\pi Dt)^{-1/2} \exp[-x^2/2Dt]$. In the above we assumed that the reflecting boundary is located at $x = 0$. The kurtosis can be found by calculating the expressions for moments $C_n = \int_0^\infty dx (x - x_0)^n G(x; x_0, t)$ with $n = 2, 4$. The moments have to be then averaged over the value of x_0 , that we assume to be uniformly distributed in the region $0 < x < L$ with $L \gg \sqrt{Dt}$ being a characteristic compartment size. Straightforward integration yields the following expressions for the moments in the leading order over \sqrt{Dt}/L : $C_2 = Dt/2 - (Dt)^{3/2}/3\sqrt{\pi}L$ and $C_4 = 3(Dt)^2/4 - 4(Dt)^{5/2}/5\sqrt{\pi}L^2$. Note that the correction to C_4 is smaller in comparison to the correction to C_2^2 which explains the initial rise of the kurtosis $K = 4(Dt)^{1/2}/15\sqrt{\pi}L$. The numerical factors in this expression are not universal and may depend on the actual form of the compartment. However, the scaling laws $K \propto t^{1/2}$ and $K \propto L^{-1}$ are universal, they are seen in the inset of Figure 2 and can be checked experimentally. Qualitatively the positive value of the kurtosis at small times $t \ll \tau_d$ can be explained as follows: randomly choosing the initial position of the particle inside the compartment we will observe at short times the Gaussian fluctuations of the displacement for the initial positions away from barriers and super-Gaussian fluctuations for the initial positions near barriers (motion downhill in the potential is super-Gaussian).

For intermediate timescales $\tau_d \ll t \ll \tau_h$ the particle has enough time to diffuse around its compartment, however the events of passing through the barrier are still rare. In this regime one can calculate the value of the kurtosis by assuming that the Green function $G(\mathbf{r}; \mathbf{r}_0, t) = P_\infty(\mathbf{r})$, where $P_\infty(\mathbf{r})$ is the uniform distribution with support inside the compartment. This assumption implies that the particle had enough time to explore the whole compartment, and moreover, that the width of the barriers is negligible in comparison to the compartment size. If the later approximation is not justified, the Green function has to be replaced by equilibrium Boltzmann-type distribution $G(\mathbf{r}; \mathbf{r}_0, t) = \exp[-U(\mathbf{r})/T]/Z$. As long as the initial particle position is also uniformly distributed over the compartment we obtain the following expressions for the moments of particle jumps: $C_n = \int_C d\mathbf{r} \int_C d\mathbf{r}_0 (\mathbf{r} - \mathbf{r}_0)^n P_\infty(\mathbf{r}) P_\infty(\mathbf{r}_0)$ that yields $K(t) = -1/10$ for triangular compartments with very thin barriers. Figure 3 shows that the position of the kurtosis minima indeed scales as L^2 , i.e. as the diffusion scale. Note that we observed from simulations that the value of the kurtosis on these timescales is sensitive to the actual shape of compartments and to the width of the barrier potentials. It suggests that the kurtosis might be used for getting experimental insight on these membrane properties. The change of kurtosis sign shows that the first peak is observed at the time-scales comparable to τ_d which suggests a way of inferring the size of the compartment from the position of first peak (assuming that the diffusion coefficient is known from the MSD analysis). Qualitatively the decrease of the kurtosis for $t \sim \tau_d$ can be explained as follows: t in that case

is large enough for the particle from any initial position inside compartment to hit the barrier. However, the time $t \sim \tau_d$ is not sufficient to expect jumps over barrier so that the fluctuations of the particle displacement are sub-Gaussian.

The late time asymptote $t \sim \tau_h$, that is responsible for the second peak of the observed kurtosis, is determined by trajectories that have a finite number of hops between the compartments. The non-Gaussianity of the jump distance distribution is related to the discrete nature of barrier hopping events. When the typical number of hopping events is small, say 1 – 2, the fluctuations of the total distance traveled by a particle are stronger than Gaussian (because after each jump over the barrier the particle typically moves away from the barrier), and that explains the rise of the kurtosis at $t \sim \tau_h$. As the number of hops becomes very large for $t \gg \tau_h$, the distribution becomes Gaussian again, due to central limit theorem. The kurtosis decays back to zero as τ_h/t . For the analytical estimate of the position of the second peak we look at square compartments of size L and assume that at $t \gg \tau_d$ the density inside the initial compartment is almost constant. We then assume that the perturbations above that constant have a form of the quadratic polynomial in x and y with the same approximation for the four neighboring compartments (i.e. we neglect the probability of secondary jumps into more distant compartments). Using the boundary condition (3) between compartments (integrated along each boundary) we obtain the time dependence of p in every compartment. Calculating the kurtosis (1) from that solution we obtain the position of the second kurtosis peak $\tau_{peak,2}$ as follows

$$\tau_{peak,2} = \frac{\mathcal{P}^{-1}L}{5D} \ln \frac{6}{5} + O\left(\frac{L^2}{D}\right), \quad (4)$$

there $O\left(\frac{L^2}{D}\right)$ term could be roughly estimated as the initial equilibration time of the particle in the compartment L^2/D . Figure 7 compares the dependence of the position of the second kurtosis peak for the square compartments of size L obtained numerically with the fit to the expression (4) assuming $O(L^2/D) = \alpha L^2/D$ and the fitting parameter value $\alpha = 1.216$. Note the applicability of the analytical expression (4) requires that $\frac{\mathcal{P}^{-1}L}{5D} \gg L^2/D$ which is not well satisfied for the parameters $\sigma = 5\text{nm}$ and $H = 7$ and typical values of L in Figure (4) (applicability is better for smaller values of L). These numerical values were chosen to approach the typical conditions for the proteins (lipids) motion in compartments [10].

To conclude, we have proposed and analyzed a novel particle-tracking approach for the identification of nonlinear interactions. Unlike common MSD techniques, our approach is based on the analysis of the time dependence of the non-Gaussian characteristics of the particle dynamics, specifically the kurtosis of the displacement probability distribution. The functional dependence of the kurtosis on the measurement time carries a lot of information about the nonlinear interactions that con-

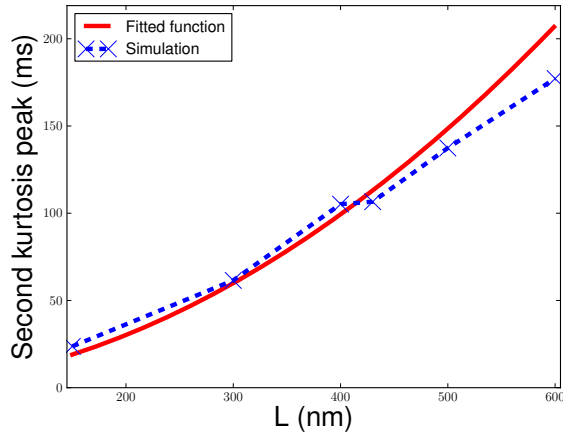


FIG. 7: (Color online) Dependence of the position of the second kurtosis peak for the square compartments of size L from simulations (crosses connected by dashed lines) vs. the dependence (4) with $O(L^2/D) = 1.216 L^2/D$ (solid line). The default parameter values $\sigma = 5\text{nm}$ and $H = 7$ are used.

tribute to the particle motion. E.g., if a particle is placed in a cage-type potential induced by cytoskeleton or transmembrane proteins, the resulting kurtosis of the displacement is a non-monotonous function with three distinct regions characterized by the change of the sign of the kurtosis slope. Specific structure of the kurtosis function depends on the characteristics of the potential: shape and size of the individual cells, heights and widths of the barriers but the change of sign feature is quite robust to the specifics of the potential. Also we would like to stress that the measurement of time-independent kurtosis as was made e.g. in Ref. [19] would not give any essential information about compartments because it would mean the averaging of the kurtosis over the horizontal axis in Figures 2 and 4 which would completely erase the change of the sign of the kurtosis slope feature which is a core idea of this Letter.

Work of P.L. was supported by NSF grant DMS 0719895. Part of the work was done, while K.T. was employed by Los Alamos National Laboratory and P.Š. by New Mexico Consortium.

-
- [1] M. J. Saxton, Nat. Methods **5**, 671 (2008).
 - [2] M. J. Saxton, and K. Jacobson. Annu. Rev. Biophys. Biomol. Struct., **26**, 373 (1997).
 - [3] R. Metzler, J. Klafter, Physics Reports **339**, 1-77 (2000).
 - [4] S. Coscoy, E. Hugueta, and F. Amblard, Bull. Math. Biol., **69**, 2467 (2007).
 - [5] S.J. Singer, and G.L. Nicolson. Science **175**, 720 (1972).
 - [6] P.G. Saffman, M. Delbrück. Proc. Natl. Acad. Sci. USA **72**, 3111 (1975).
 - [7] D.M. Engelman, Nature, **438**, 578 (2005).
 - [8] B. Alberts, *Molecular Biology of the Cell*, 5 edition (Garland Science, NY, 2007).
 - [9] D. Lingwood, and K. Simons, Science, **327**, 46 (2010).
 - [10] A. Kusumi, *et. al.*, Ann. Rev. BioPhys. Biomol Struct., **34**, 351 (2005).
 - [11] F. Daumas, *et. al.*, Biophys. J., **84**, 356 (2003).
 - [12] B. F. Lillemeier, *et. al.*, Proc. Nat. Acad. Sci., **103**, 18992 (2006).
 - [13] M.J. Murcia, *et. al.*, J. Amer. Chem Soc., **130**, 15054 (2008).
 - [14] T.G. Mason, and D.A. Weitz, Phys. Rev. Lett. **74**, 1250 (1995).
 - [15] P.W. Fok, and T. Chou, Proc. Roy. Soc. A, **466**, 3479 (2010).
 - [16] J.-B. Masson, *et. al.* Phys. Rev. Lett., **102**, 048103 (2009).
 - [17] T. Auth, and N.S. Gov, Biophys. J., **96**, 818 (2009).
 - [18] A. Kusumi, Y. Sako, and M. Yamamoto, Biophys. J. **65**, 2021 (1993).
 - [19] V. Tejedor, *et. al.*, Biophys. J., **98**, 1364 (2010).
 - [20] J. Jeon, *et. al.*, Phys. Rev. Lett. **106**, 048103 (2011)
 - [21] A. V. Weigel, *et. al.*, Proc. Natl. Acad. Sci. USA **108**, 6438-6443 (2011).
 - [22] W. Ying, G. Huerta, S. Steinberg, and M. Zúñiga, Bull. Math. Biol., **71**, 1967 (2009).